Current Research in Food Science 5 (2022) 1342–1351

Contents lists available at ScienceDirect

Current Research in Food Science

journal homepage: www.sciencedirect.com/journal/current-research-in-food-science

Wheat gluten proteins phosphorylated with sodium tripolyphosphate: Changes in structure to improve functional properties for expanding applications

Fei Hu [a], Peng-Ren Zou [a], Fan Zhang [a], Kiran Thakur [a,b], Mohammad Rizwan Khan [c], Rosa Busquets [d], Jian-Guo Zhang [a,b], Zhao-Jun Wei [a,b,*]

[a] School of Food and Biological Engineering, Hefei University of Technology, Hefei, 230601, China
[b] School of Biological Science and Engineering, Collaborative Innovation Center for Food Production and Safety, North Minzu University, Yinchuan, 750021, China
[c] Department of Chemistry, College of Science, King Saud University, Riyadh, 11451, Saudi Arabia
[d] School of Life Sciences, Pharmacy and Chemistry, Kingston University London, Kingston Upon Thames, KT1 2EE, Surrey, England, UK

ARTICLE INFO

Handling editor: Dr. Quancai Sun

Keywords:
Phosphorylation
Wheat gluten proteins
Functional properties
Solubility
X-ray photoelectron spectroscopy

ABSTRACT

Poor solubility of wheat gluten proteins (WG) has negative impact on functional attributes such as gelation and emulsification, which limits it use in the food industry. In this study, WG underwent different degrees of phosphorylation using sodium tripolyphosphate (STP). Phosphoric acid groups were successfully incorporated in the WG via covalent bonding (C–N–P and C–O–P) involving hydroxyl and primary amino groups from WG. The introduction of phosphoric acid groups increased the negative charge of phosphorylation-WG, which caused the enhancement of electrostatic repulsion between proteins and reduced the droplet size in emulsions, thereby allowing proteins to be more efficiently dispersed in the solution system. The change of structure induced with phosphorylation improved hydration of protein, making the WG with higher solubility, thereby resulting in the improvement of its emulsification, foaming, thermal stability, and rheological properties. Therefore, WG can be modified by phosphorylation which caused an overall improvement of functional properties, thus facilitating the expansion of WG applications.

1. Introduction

Wheat gluten proteins (WG) is a by-product of wheat flour separating from starch and other substances soluble in water (Shi et al., 2021). WG is recognized as a superior quality plant-based protein which composition includes many necessary amino acids, and it is nutritious, safe and inexpensive compared with most proteins (Rombouts et al., 2019; Wang, 2020). Natural WG contains great amounts of glutamines, proline, non-polar amino acids with fewer charged amino acids. Some of amino acids' side chains are prone to form hydrogen bonding or participate in interacting with hydrophobic residues (P. S. Li et al., 2020; Ortolan et al., 2022). Overall, WG has poor solubility in water that results in poor functional properties, such as emulsifications, foaming and gelation, which are not competitive with other vegetable proteins that has greater aqueous solubility (Wang, 2020). Hence, WG's unsatisfactory physicochemical properties has limited its application in the food and biomedical fields (D. Wang et al., 2021). Therefore, there is a need for modifying WG in order to improve its solubility and resulting functional attributes to obtain specific products of WG that meet the needs of different industries.

Plant proteins have been modified by using chemical, physical, and biochemical methods to transform the interaction between amino acid residues of proteins (Gultekin Subasi et al., 2021). This led to changes in the spatial structure of proteins and physicochemical properties that affect their applications (He et al., 2019). Physical modifications to change the spatial structure and intermolecular aggregation of proteins was carried out by modest thermal denaturation, mechanical treatment, and ultrasounds (Liu et al., 2021). However, physical modifications have high equipment demand, which is difficult to apply in large scale for industrial applications. In contrast, enzymatic modifications are highly specific and need mild reaction conditions, however it might not be feasible to adopt because they require certain costly pre-treatments.

* Corresponding author. School of Food and Biological Engineering, Hefei University of Technology, Hefei, 230601, China.
E-mail addresses: hufei@hfut.edu.cn (F. Hu), 1040744976@qq.com (P.-R. Zou), zffs2012@mail.ahnu.edu.cn (F. Zhang), kumarikiran@hfut.edu.cn (K. Thakur), mrkhan@KSU.EDU.SA (M.R. Khan), r.busquets@kingston.ac.uk (R. Busquets), zhangjianguo@hfut.edu.cn (J.-G. Zhang), zjwei@hfut.edu.cn (Z.-J. Wei).

https://doi.org/10.1016/j.crfs.2022.08.014
Received 22 July 2022; Received in revised form 13 August 2022; Accepted 22 August 2022
Available online 28 August 2022

Chemical modifications are still the mainstream direction of protein modification because of their low cost or equipment requirements, significant effect and short reaction time.

Chemical modifications such as phosphorylation, acylation, glycosylation and deamidation made it possible to insert functional groups in proteins (Abedi and Pourmohammadi, 2021; Busra et al., 2021). Among these, phosphorylation was a valid approach for upgrading the functional properties of food proteins. The specific reactive groups of protein side chain were susceptible to participate in reaction, such as the hydroxyl groups of Threonine (Thr), Serine (Ser), Tyrosine (Tyr) and the ε-amino groups of Lysine (Lys), which can react with phosphate groups to become (Thr, Ser) Tyr-$PO3^{2-}$ and Lys- $PO3^{2-}$, thereby introducing a large number of phosphate groups. There were a large number of negatively charged phosphoric acid groups in phosphorylated proteins, which significantly altered the electronegativity of proteins surface and enhanced the electrostatic repulsion between proteins (Ai and Jiang, 2021). Those changes make it easier to disperse into water, thus affecting the functional properties of protein. There are common types of phosphorylation agents for protein modification, such as phosphorus oxychloride ($POCl_3$), P_2O_5/H_3PO_4, sodium tripolyphosphate (STP) and cyclic trisodium phosphate (sodium trimetaphosphate, STMP). Among these, the STP is a food additive by FDA approving with the virtues of easy handling, low price and safety (Zou et al., 2022a). From a toxicological point of view, WG modifications with STP are safe and feasible.

Recent studies have modified rice bran protein, ovalbumin, walnut isolate protein, and mung bean protein via phosphorylation. For instance, Hu et al. (2019) found that the phosphorylation of rice bran protein caused changes in its conformation; It was unfolded and showed greater flexibility, passing from originally insoluble agglomerates to soluble components, thereby ameliorating the water solubility of protein and emulsifying activity. Although the food proteins modified by phosphorylation has been studied for the past few years, studies on WG phosphorylation are still novel. Therefore, there is a need to comprehensively understand the structural variation during phosphorylation modification that appears in WG and their effects on the functional characteristics of WG. Consequently, the aim of this research was to prepare phosphorylated WG (PP-WG) using sodium tripolyphosphate to explore the connection between functional properties and structural changes. This study will facilitate the utilization of WG sources in the biomedical and food field.

2. Materials and methods

2.1. Materials

Wheat gluten was purchased from Anhui Ant food Co., Ltd (Suzhou, China). Sodium tripolyphosphate (STP) was purchased from Shanghai Maclin Biochemical Technology Co., Ltd. of China. The chrome black T was provided by Aladdin Biochemical Technology Co., Ltd (Shanghai, China). Bradford protein assay Kit was brought from Biyuntian Biotechnology Co., Ltd (Shanghai, China). The dialysis bag was obtained from Yuanye Biotechnology company (Shanghai, China), which the molecular weight cut-off is 500–1000 MW. The rest of analytical grade chemicals in this work were provided by Shanghai Sinopharm Chemical Reagent Co., Ltd from China.

2.2. Extraction of WG

Wheat gluten is mainly composed of about 75% (w/w) protein, a certain amount of wheat starch, cellulose and lipids. Although the protein content of wheat gluten is already high, in order to avoid the influence of the contained oil and polysaccharide impurities on the subsequent spectral detection and determination of functional properties, this study used the alkali-soluble acid precipitation method to extract the protein. Wheat gluten proteins (WG) were extracted from wheat gluten powder basing on a described approach of Arte et al. (2019) and Chai et al. (2020) with some modifications. Briefly, after dispersing the wheat gluten powder with deionized water to obtain a 10% dispersion (w/v), the pH of dispersion was regulated to 12 with 1 M NaOH and then stirred for 2 h. The obtained dispersion was centrifuged at 10,000 rpm/min for 10 min to remove starch and other impurities. The supernatant was collected and regulated to pH 4.0 with 1 M HCl. Then the precipitated crude protein samples were collected after centrifugation at 10,000 rpm/min for 10 min. The wheat gluten proteins (WG) were obtained after washing the precipitate three times with deionized water to remove salt. The protein content of resulting WG sample was 87.9%, which was determined by the Kjeldahl Nitrogen Determination method.

2.3. Preparation of phosphorylated WG

The phosphorylated WG (PP-WG) was prepared by referring the method described by Yan and Zhou (2021) and Zou et al. (2022b). Briefly, a quantity of WG (10 g) was dissolved in water to form a dispersion of 10% under continuous stirring. The STP was added to the WG suspension at different proportion (2%, 4%, 6% and 8%, g STP/g protein). The mixed solution was adjusted to pH 9.0 with 1 M NaOH, which was maintained to pH 9.0 by intermittent addition of NaOH solution under reaction time of 3 h at 45 °C. The reaction was then end by cooling to room temperature. The pH of solution after ending reaction was brought to 7.0 with the addition of 1 M HCl. Finally, the extra STP was eliminated by dialyzing the suspension for 48 h. The phosphorylated WG was gained from the precipitates, which the suspension after dialysis was centrifuged for 10 min at 4500 rpm/min to remove the supernatant. The phosphorylated WG was named to PP-WG-2%, PP-WG-4%, PP-WG-6% and PP-WG-8% according to the added amount of sodium tripolyphosphate.

2.4. Determination of phosphorylation degree of PP-WG

The phosphorylation extent of PP-WG was evaluated by ethylenediaminetetraacetic acid (EDTA) titration as previously reported by Zhang et al. (2007) with some modifications. Briefly, 5 mL of solution was taken before and after the phosphorylation reaction (as mentioned above Section 2.3), and mixed with trichloroacetic acid (5 mL, 10%) to denature the protein and precipitate. The suspension was centrifuged to obtain the supernatant (4 °C, 4000 rpm, 10 min). The pH of supernatant was regulated to 3.8–3.9 by adding 1 M zinc acetate to achieve precipitation. The precipitate zinc pyrophosphate ($Zn_2P_2O_7$) was formed after adding zinc acetate. Ammonia solution was added to dissolve the precipitate, and then the mixed solution was titrated by adding 0.2 M EDTA (C, mol/L) with chrome black T as an indicator. The titration end point was when the color of aqueous changed from purple-red to blue, and the V_1 and V_2 (expressed in L) were the volumes of EDTA that was consumed by the blank sample and PP-WG samples. The phosphorylation degree (DP) was counted as the following equation (1):

$$DP = \frac{C \times (V_1 - V_2) \times Mp}{2m} \quad \text{Equation 1}$$

Where m is the mass of WG in the sample (expressed in grams); Mp is 30.97 g/mol (the relative atomic mass of phosphorus).

2.5. Structural characteristics of PP-WG

2.5.1. Fourier transform infrared spectroscopy (FT-IR) analysis

FT-IR spectroscopy analyses were carried out by the Nicolet 6700 spectrometer (Thermo Fisher, USA) with a diamond ATR (attenuated total reflectance method) accessory under the method described by Yu et al. (2022) and Duarte et al. (2022) with some modifications. The samples were scanned at a resolution of 4 cm^{-1} and full wavelength (650-4000 cm^{-1}) with 32 scans. Each sample was scanned for 3 times.

2.5.2. Surface chemical composition analysis

Surface chemical composition of WG and PP-WG samples were characterized by the ESCALAB250Xi X-ray photoelectron spectrometer (XPS) (Thermo Fisher, USA) equipped with Al K-alpha radiation X-rays of 300 W and monochromatic Kα source (hν = 1486.6 eV, 250 W) basing on the approach as described by Wehrli et al. (2021). The spectrum of each element was determined with a resolution of 0.05 eV and pass energy was 25 eV. All spectra (binding energy and photoelectron yield intensity) were recorded through a double anodic Al target as the following order: survey, P2p, C1s, N1s, and O1s. The curve peak of C1s was analyzed to obtain decomposition peak by XPS Peak Fit software.

2.5.3. Crystal structure analysis

The crystal structure of protein samples was characterized by the X-ray diffractometer (XRD) (D/MAX 2500 V, Rigaku Corporation, Japan) with Cu-Kα radiation (k = 1.5406 Å) according to the approach as described by (Hadidi et al., 2021). Each sample was observed at a speed of 2°/min in the diffraction angle range that covered all substantial diffraction peaks from 5° to 35° (2θ). The data was analyzed by MDI Jade 6.0 software.

2.5.4. Surface morphology characterization

The microstructure of WG and PP-WG samples was observed by scanning electron microscope (SEM) (Regulus 8230, Hitachi, Japan) under the approach reported by Shamsudin et al. (2022) with minor modifications. Each sample was fixed on double-sided conductive adhesive and sprayed with gold under vacuum. The morphology of gold-plated samples was observed with an accelerating voltage of 15 kV at a magnification of 300× and 1000x.

2.6. Physicochemical properties of PP-WG

2.6.1. Zeta potential

The zeta potential of protein samples was determined at room temperature by a Zeta sizer of Nano-ZS (Malvern Ltd, UK) basing on the description of Li et al. (2022). The freeze-dried WG and PP-WG samples were dissolved to obtain a final concentration of 0.05% (w/v, the solution is phosphate buffer (pH 7.0)). Each sample was carried out in triplicate.

2.6.2. Particle size distribution

The distribution of particle size for WG and PP-WG samples was determined using a laser particle size instrument of Mastersizer-2000 (Malvern Ltd, UK) basing on previous reference (Farooq et al., 2022). After the instrument was calibrated with blue light, samples were added when the light transmission was 75% or more, and measurements started when the sample shading was 8%. The measure medium was water.

2.6.3. Dynamic rheological measurement

The rheological attributes of WG and PP-WG samples were characterized by means of a rheometer of DHR-3 (TA Instruments Co., Ltd., USA) (J. Zhao et al., 2022). The parallel plate geometry of 40 mm diameter was equipped to the rheometer. The shear behavior of protein solution (10%, w/v) was measured at 25 °C from the shear speed range of 0.01–100 s^{-1}. The assay conditions were set as follows: the gap between sample and parallel plate was adjusted to 0.05 mm and a fixed stress of 1%. The flow curve was plotted as a logarithmic function of apparent viscosity against shear rate. A frequency scan was then performed on the protein solution (10%, w/v) with the strain set to a constant value of 1% (in the linear viscoelastic region) to measure the storage and loss modulus (G′ and G″) at 25 °C from 0.01 to 10 Hz.

2.6.4. Thermogravimetry (TGA) analysis

The thermal properties of protein samples were measured using the STA449C thermogravimetric analyzer (NETZSCH Co., Ltd., Germany) by following previous approach (Marangoni et al., 2022). Approximately 8 mg of the freeze-dried WG and PP-WG samples was heated to 600 °C from 30 °C at 10 °C/min.

2.7. Functional properties of PP-WG

2.7.1. Solubility

The Coomassie brilliant blue method was carried out to measure solubility of protein (D'Amico et al., 2015). A standard curve was first plotted with the concentration of bovine serum albumin as the independent variable and the absorbance value at 595 nm was the response or dependent variable. The samples of WG and PP-WG were dissolved in deionized water to form a protein dispersion (1%, w/v) and stirred magnetically for 2 h to fully hydrate at room temperature, then the dispersion was centrifuged at 3500 rpm for 15 min to obtain the supernatant. The content of protein in solutions was measured by the Bradford method. Briefly, 5 μL of supernatant was pipetted into the sample wells of a 96-well plate then added 250 μL of G250 staining solution. The absorbance of each solution was measured using an enzyme marker (PT-3502B, Potenov, China) at 595 nm. The solubility percent of protein was counted according to equation (2):

$$Solubility\ (\%) = \frac{C1}{C2} \times 100\% \qquad \text{Equation 2}$$

Where C1 is the protein concentration of supernatant, g/mL; C2 is the added amount of WG in initial solution, g/mL.

2.7.2. Water holding capacity (WHC) and oil absorption capacity (OAC)

The water/oil holding capacities of WG and PP-WG samples were measured following a method by Z. M. Wang et al. (2021) and X. Y. Li et al. (2021) with minor modifications. Briefly, 5 g of distilled water/oil (W_1/O_1) were added to each protein sample (0.5 g, M). The mixed solution was whisked for 1 h, and then centrifuged at 3000 rpm for 15 min after standing for 20 min at room temperature. The mass of the supernatant (W_2/O_2) was weighed. The WHC and *OAC* were calculated as equation (3) and equation (4):

$$\text{WHC}\ \ (\text{g water / g protein}) = \frac{(W_1 - W_2)}{M} \qquad \text{Equation 3}$$

$$\text{OAC}\ \ (\text{g oil / g protein}) = \frac{(O_1 - O_2)}{M} \qquad \text{Equation 4}$$

2.7.3. Emulsion activity index (EAI) and emulsion stability index (ESI)

The EAI and ESI of WG and PP-WG samples were measured with an approach described elsewhere (L. Wang et al., 2017). Briefly, 0.2% (g/mL) protein dispersion (protein dissolved in phosphate buffer (0.2 M, pH 7.0)) and 5 mL soybean oil were blended by high pressure homogenizers for 3 min at 15,000 rpm/min. The emulsion was drawn from the bottom of vessel (0.5 mL) after emulsion formation at 0 and 10 min, and then 5 mL of the SDS solution (0.1%, w/v) was added to incubate with the emulsion. The absorbance of mixture was determined by a UV–Vis spectrophotometer of (UV-4802, UNICO, USA) at 500 nm after the emulsion was incubated with SDS solution. EAI and ESI were counted with reference to equation (5) and equation (6):

$$EAI\ (m^2/g) = \frac{2 \times 2.303 \times A_0 \times N \times 10^{-4}}{\varnothing LC} \qquad \text{Equation 5}$$

$$ESI\ (min) = \frac{A_0}{A_0 - A_{10}} \times 10 \qquad \text{Equation 6}$$

Where N is the dilution used (100); φ is the fraction of the system accounted for by the oil phase, which in this test was 0.25; L is the light diameter of colorimetric pool (0.01 m); C is the concentration of protein (g/mL); A_0 and A_{10} are the absorbance of emulsion at 0 and standing for 10 min after incubating with SDS.

2.7.4. Foam capacity (FC) and foam stability (FS)

The FC and FS of WG and PP-WG samples were measured basing on the described approach of Zheng et al. (2022). Protein sample was dispersed in 0.2 M phosphate buffer (pH 7.0) to get protein suspension (1%, w/v), and then followed by homogenization (15,000 rpm for 3min). The FC and FS were counted with reference to equation (7) and equation (8):

$$FC = \frac{V_0 - V}{V} \times 100\% \quad \text{Equation 7}$$

$$FS = \frac{V_{30} - V_0}{V_0 - V} \times 100\% \quad \text{Equation 8}$$

where V is the volume of protein suspension before homogenization; V_0 and V_{30} are the volume of protein solution at 0 and standing for 30 min after homogenization.

2.8. Statistical analysis

All the determination were repeated in triplicate and data were processed and analyzed by SPSS software. The results were represented as mean ± SD. Meanwhile statistical analysis was performed by one-way analysis of variance with Duncan test, $p < 0.05$.

3. Results and discussion

3.1. Effect of STP concentrations on the phosphorylation of WG

The phosphorylated reaction of protein could take place between the hydroxyl groups of amino acids of Thr, Ser, Tyr or the ε-amino group of Lys and phosphate groups. The WG was modified by hydrothermal phosphorylation using different STP concentrations and the resulting phosphorylation degree of phosphorylated WG was shown in Fig. 1A. It had been found that the degree of phosphorylation tended to increase approximately linearly as the STP concentration increased from 0 to 10%. As the STP concentration further increased, the percentage of phosphorylation with WG declined. These results were in agreement with what was found for the phosphorylation of soybean isolate proteins by STP. In that case, the phosphorylation degree declined from the STP concentration of 9% (Zhang et al., 2007). The sudden decline of phosphorylation could be because when the amount of phosphate groups was raised to a certain level, the electrostatic repulsion and steric effect produced between the phosphorylated protein molecules and the excess phosphate groups became detrimental to phosphorylation (Q. L. Zhao et al., 2022).

3.2. Changes in functional groups or chemical bonds for PP-WG

The FT-IR spectra of natural and phosphorylated WG were shown in Fig. 1B. It can be observed the high similarity between the spectra from WG and derivatized proteins. There were key differences in raw and phosphorylated WG, such as the absorption bands of 1600–1700 cm^{-1}, which potentially due to the vibrational frequency of amide I ascribed to the nature of hydrogen bond between the N–H and C═O (Zhang et al., 2021). The peak of PP-WG displayed a weakness in the peak intensity at the amide I band compared to the raw WG, suggesting that the secondary structure of WG was altered by phosphorylation modification. Two new feature peaks emerged for PP-WG at wavenumbers of 1105.1 and 897.2 cm^{-1}, which could belong to the stretching of P═O and P–O, respectively. However, the spectrum of raw WG had almost no peaks at these positions compared with phosphorylated WG, implying that phosphoric acid groups were introduced to WG after phosphorylation, thereby resulting in alteration of protein structure. This phenomenon might be due to that the hydrogens of the –OH groups of Ser were replaced by the phosphate groups of STP during phosphorylation. The absorption band at 897.2 cm^{-1} could belong to C–O–P. Furthermore, the

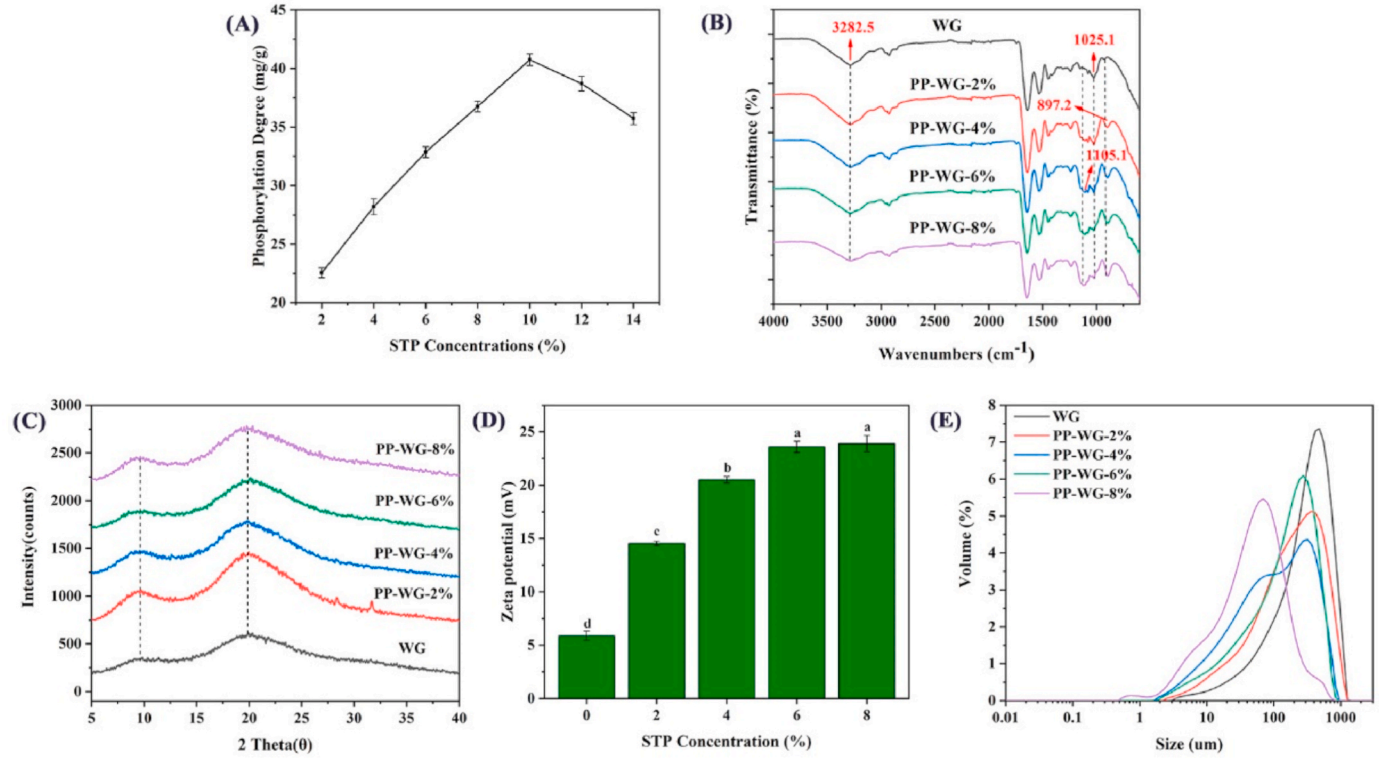

Fig. 1. Degree of phosphorylation of wheat gluten modified with different sodium tripolyphosphate concentrations (A). Fourier transform infrared spectra (B); X-ray diffraction spectra (C); Zeta potential (D); and particle size distribution of native and phosphorylated wheat gluten samples (E). The error bars and "a-d" in D correspond to PP-WG and WG, respectively. WG indicates wheat gluten proteins. PP-WG indicates phosphorylated wheat gluten proteins.

absorption band at 3300-2900 cm^{-1} was attributed to the stretching vibration of –OH and N–H. It was observed that the band intensity at 3300-2900 cm^{-1} was weaken in the PP-WG sample compared to raw WG sample, which could be possible because of attachment of phosphoric acid groups to the –OH and $–NH_2$. Xiong et al. (2016) reported that the FT-IR spectra was consistent with phosphoric acid groups having been introduced in ovalbumin molecule by the reaction of amino acid esterification during phosphorylation. Taken together, the above results can infer that the C–O–P and C–N–P bonds may produce between the STP and WG after phosphorylation reaction.

3.3. Introduction of phosphate groups in PP-WG

To further determine the binding of phosphate to proteins, the XPS was adopted to characterize the presence of P elements and the surface properties of protein. The survey spectra and chemical states of C1s and P2p in raw and phosphorylated WG by peak fitting were shown in Fig. 2. As can be observed from Fig. 2A, the peaks were located at ~531.9, ~399.7, ~284.8 and ~133.1 eV corresponded to O1s, N1s, C1s, and P2p respectively. As shown in Fig. 2B, the P2p peak of 133.1 eV was clearly detected in the PP-WG samples, but this peak was barely detected in the raw WG, which confirmed that phosphorylation successfully introduced phosphate groups to the surface of WG molecule. This result was consistent with the FT-IR results. According to the binding energy of

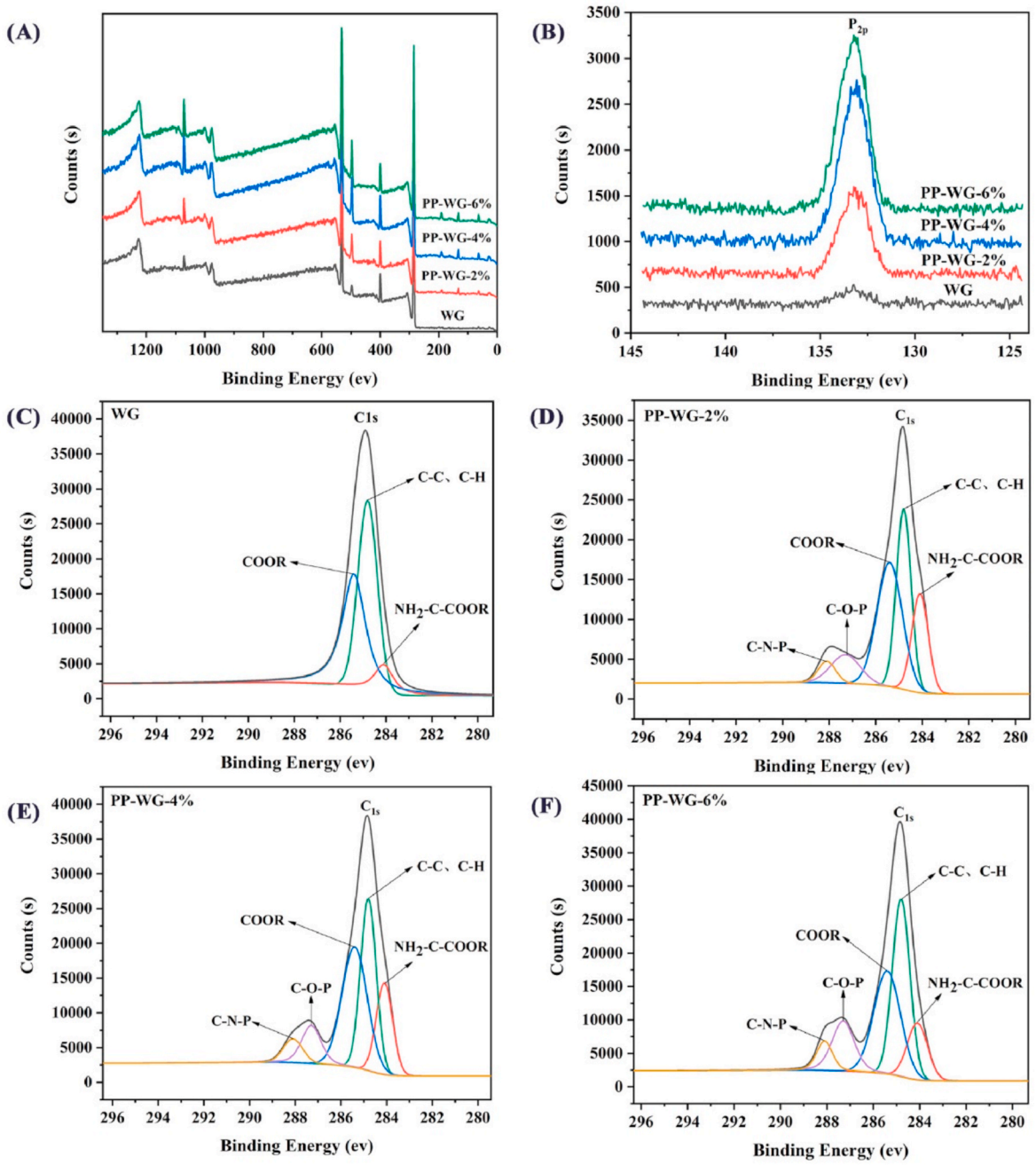

Fig. 2. X-ray Photoelectron Spectra of native and phosphorylated WG samples (A); peaking fitting spectra of P_{2P} in native and phosphorylated WG samples (B); Peaking fitting spectra of C_{1S} in native (C), Peaking fitting spectra of C_{1S} in PP-WG-2% (D), peaking fitting spectra of C_{1S} in PP-WG-4% (E) and peaking fitting spectra of C_{1S} in PP-WG-6% (F). PP-WG-2%, PP-WG-4% and PP-WG-6% indicate that wheat gluten proteins are phosphorylated at different adding proportion of sodium tripolyphosphate (2%, 4% and6%, g STP/g protein).

carbon bonds in the WG and PP-WG, the C1s photoelectron peaks were decomposed, which was displayed in Fig. 2C–F. The peaks of binding energy at~285.4 eV, ~284.8 eV and ~284.1 eV belonged to C–C (or C–H), COOR, C–N, respectively. As shown in Fig. 2D–F, the decomposed peaks of C1s spectra in phosphorylated WG led to discovering two new peaks at ~288.1 and ~287.3 eV, which matched with C–N–P and C–O–P bonds, respectively (Yang et al., 2019). However, it was not found in the C1s decomposed peaks of raw WG from Fig. 2C. Both $-NH_2$ on the side chains of arginine and lysine residues and –OH on the side chains of threonine and serine residues in plant proteins have been reported to exhibit the high activity, which can react with phosphoric acid groups during phosphorylation modifications (Li et al., 2009). Thus, the formation of C–O–P and C–N–P bonds between the STP and WG after phosphorylation was confirmed, which was consensus with a preceding reported result (Xiong et al., 2016).

3.4. Changes in crystal structure of PP-WG

XRD was widely adopted for crystal structure analysis, which can be applied to study alterations in crystal structure of protein before and after physical and chemical modifications. The XRD spectra of WG before and after phosphorylation modification were illustrated in Fig. 1C. The diffraction intensity and diffraction angle (2θ) were associated to the crystal size: the bigger diffraction angles and the lower diffraction intensity with the smaller crystal size. It can be seen from figure that two most prominent diffraction peaks existed in the spectra of all samples at approximately $2\theta = 20°$and $2\theta = 10°$, which could respectively belong to the crystalline region II and I. It was found that the FWHM peak (full width at half maximum) of all phosphorylated WG became small compared to the natural WG. Meantime, the diffraction peak intensity of all phosphorylated WG became enhanced compared to raw WG, indicating that the crystallinity of WG changed owing to the interaction of the phosphoric acid groups with proteins. In addition, the diffraction peak of phosphorylated WG samples at $2\theta = 20°$ was observed to shift to a higher angle compared to the diffraction peak of WG. These results suggested that the WG has been modified by phosphorylation to create new chemical bonds in protein molecule. The regular arrangement of WG molecules was disrupted during phosphorylation modifications and it reduced the overall rigidity and led to smaller crystal sizes, which was in agreement with the reported results of Yu et al. (2015).

3.5. Changes in surface morphology for PP-WG

The morphology of WG before and after phosphorylation was exhibited in Fig. 3. The SEM revealed that the particles of WG were aggregated (Fig. 3A). Furthermore, the particle surfaces of WG were relatively smooth. However, as shown in Fig. 3B–E that the particles of phosphorylated WG exhibited some cracks and fragments, indicating that the phosphorylation disrupted the initial dense aggregated state. The particle surfaces of phosphorylated WG became rough and presented porous structure compared with raw WG. The charge repulsion between proteins was enhanced due to the introduction of phosphoric acid groups, which resulted in that proteins were less prone to aggregation, changing the structure of phosphorylated WG. These results suggested that phosphate esterification occurred during phosphorylation modification (Shi et al., 2017).

3.6. Zeta potential

Zeta potential can explain the degree of the mutual repulsion or attraction between the charged protein particles (Yang et al., 2019). As shown in Fig. 1D, zeta potential's absolute value for all PP-WG sample was increased compared to raw WG and remarkably raised with increasing STP concentration. The increase of zeta potential value for PP-WG samples could be ascribed to the attachment of phosphate groups to WG molecules during phosphorylation modification, which resulted in the WG surface with more amount of net negative charge. This result was in agreement with a previous report that the zeta potential values of other plant proteins was improved by phosphorylation modification (Hadidi et al., 2021).

3.7. Particle size distribution

The changes of particle size distribution for WG after phosphorylation modification were exhibited in Fig. 1E. The particle size and distribution of proteins was very crucial factor for their functional performances. As shown in figure that the raw WG had larger particles size and narrower distribution. However, the particle size of phosphorylated WG samples had a smaller particle size distribution (the position of the peak is shifted to the left) after phosphorylation compared with raw WG. Furthermore, the distribution curve of particle size for PP-WG sample moved left as the STP concentration raised and had more wide distribution of particle size than raw WG. The introduction of phosphate groups into the WG, had resulted in the enhancement of electrostatic repulsion between protein structures thus enhancing the steric hindrance effect of particles that would not favor particle to aggregate (Hu et al., 2021). The reduction of particle size for WG by phosphorylation was in agreement with a previous report that found a remarkable reduction of phosphorylated rice gluten protein in

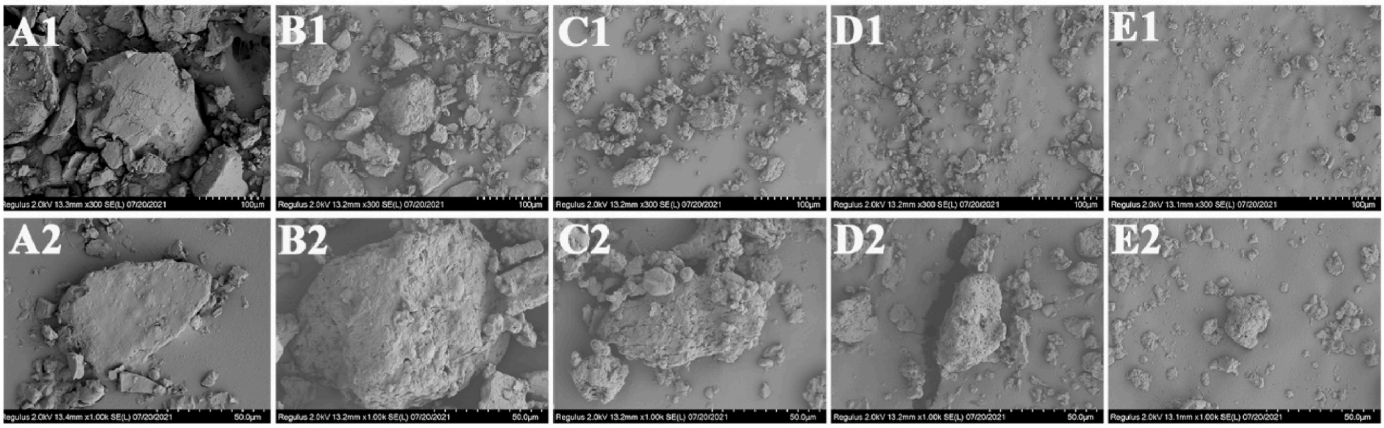

Fig. 3. Surface morphology of native and phosphorylated WG samples by Scanning electron micrographs. (A) WG; (B) PP-WG-2%; (C) PP-WG-4%; (D) PP-WG-6%; (E) PP-WG-8%. 1 and 2 indicates the magnification of images, 300 and 1000 times, respectively. PP-WG-2%, PP-WG-4% and PP-WG-6% indicate that wheat gluten proteins are phosphorylated at different adding proportion of sodium tripolyphosphate (2%, 4%, 6% and 8%, g STP/g protein).

particle size (Wang et al., 2019).

3.8. Rheological properties

The rheological properties were associated to the nature and internal structure of material, which can reflect the gelation capacity, emulsification property and other functional properties of protein. As an important indicator for the changes of intermolecular forces on proteins in aqueous system, the apparent viscosity was related to the relative molecular weight, particle size and hydration of WG. As shown in Fig. 4A, the apparent viscosity of all samples in liquid phase decreased as the shear rate increased, which exhibited typical shear thinning characteristics. The shear thinning properties of proteins can be explained by the disruption or rearrangement of entangled polymer network structure under high shear rates. At low shear rates, proteins were prone to fold and become entangled, which then resulted in more high viscosity through spatial resistance and internal dissipation within protein chain. However, at high shear rates, the speed of disrupting to entanglement between protein molecule chains was greater than the speed of reconnection, resulting in less resistance to intermolecular flow and lower apparent viscosity. The results of figure showed that the apparent viscosity of all PP-WG sample became higher compared to raw WG, suggesting that there was a large number of associations between phosphorylated WG molecules. The increase of viscosity for phosphorylated WG can be ascribed to molecular transformation induced by phosphoric acid groups. In addition, phosphoric acid groups altered surface charge of protein molecules, thus influencing the hydration layer.

To further investigate the viscoelasticity of raw and phosphorylated WG samples, frequency scan measurements were carried out. As shown in Fig. 4B and C, the storage and loss modulus (G′ and G″, respectively) of all WG samples exhibited a strong frequency dependence, which raised with increasing angular frequency. Furthermore, the G′ was remarkably higher than G″ over the sweep range of whole frequency for protein samples, indicating that protein can form a stable and strong gel network. The G′ and G″ were influenced by a variety of factors, such as the interactions of protein-protein and the flexibility of proteins. It can be observed from graph that the G′ and G″ of phosphorylated WG samples were higher than raw WG, and this trend became more significant as the STP concentration increased (Chen et al., 2020). The increase of G′ and G″ in the phosphorylated WG may be attributed to the introduction of phosphate groups, which increased physical cross-linking of protein network due to that a large number of hydrogen bonds were formed between the phosphoric acid groups and the protein. These results indicated that the flexibility of protein chains can be disrupted by phosphorylation modification, resulting in forming more elastic and viscous gels, which were consistent with a previous report (Ai and Jiang, 2021).

3.9. Changes in thermal characteristics for PP-WG

Thermal characteristic of protein was closely related to its use in food industrial applications. Thermogravimetric analysis (TGA) was widely taken to reflect the thermodynamic performances of protein and their stability. As the temperature increased, the protein sample underwent a variety of changes, including the loss of free and crystalline water, evaporation of water, unleash of small molecular volatiles or oxidative breakdown of protein. The TGA curves for freeze-dried raw and phosphorylated WG about mass loss was shown in Fig. 5A, and their derived thermogravimetric (DTG) variation curves were shown in Fig. 5B which were obtained by second order derivation. All samples showed similar thermogravimetric analysis curves (Fig. 5A), which contained the overall process of thermogravimetric decomposition for raw and phosphorylated WG. The mass loss processes were divided into two stages in the 25–600 °C. The first stage in the temperature below 200 °C was associated to the water loss of protein molecules, where the mass loss of all samples was small. For all samples, it can be observable that the temperature range of 80.12–83.71 °C was the process of moisture loss at maximum, which was due to the volatilization of bound and free water. The second stage in the 200–500 °C was related to subsequent components volatilization from proteins at the melting point, where all samples degraded rapidly with a large mass loss during thermal decomposition. This may have been caused by the disruption of interactions (intra- and intermolecular hydrogen bonds, other van der Waals forces and electrostatic interactions). The mass loss of protein samples with high degradation rate took place in the temperature range of 312.21–322.54 °C, which was similar with the results of Y. Q. Wang et al. (2017). The phosphorylated WG samples exhibited lower degradation rate and higher residual amount after pyrolysis, which implied that the thermal stability of all PP-WG sample was greater than that of raw WG. It could be a consequence of stronger binding between the phosphoric acid groups and proteins.

The DTG peaks for all samples were similar and showed flat and broad shape (Fig. 5B), suggesting that the pyrolysis of WG exhibited wide temperature range and slow rate with increasing temperature. The first endothermic peak in the DTG curves for the raw and phosphorylated WG samples corresponded to the first process of mass loss that appeared in the TGA curves, which was related with the removal of crystalline water. Presumably, the second endothermic peak in the DTG curve was correlated with melting process of protein, as they emerged before the process of mass loss in the TGA curve. Therefore, the second peak in the DTG curve matched with the second process of mass decrease in the TGA curve, which was reflective of the maximum loss rate of sample mass. It can be observed that the second peak of phosphorylated WG samples was the rightward shift compared to raw WG, which indicated that WG modified by STP exhibited more firm protein molecular backbone. These results supported that the thermal stability of WG was

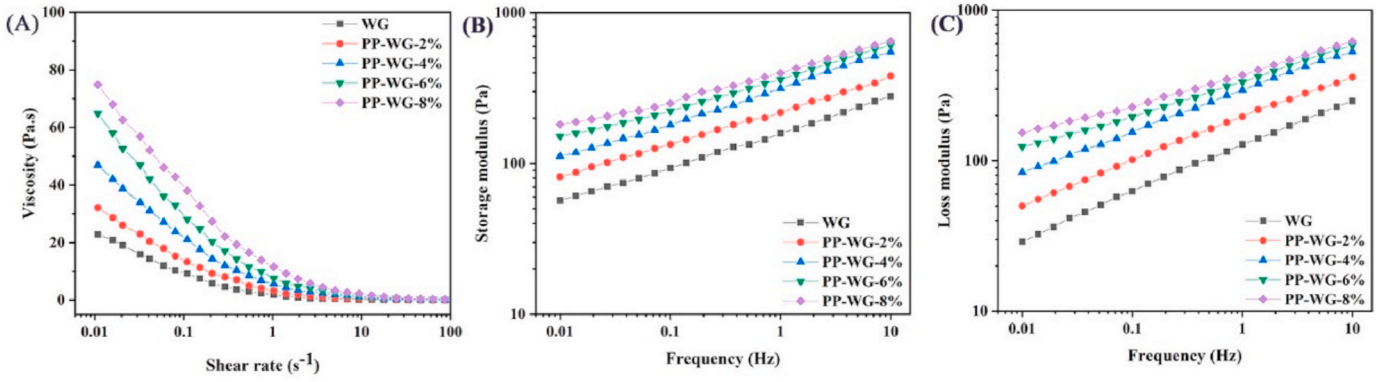

Fig. 4. Rheological measurements of native and phosphorylated WG. (A): Apparent viscosity as a function of shear rate; (B): storage modulus (G′) and angular frequency relationship; (C): loss modulus (G″) and angular frequency relationship.

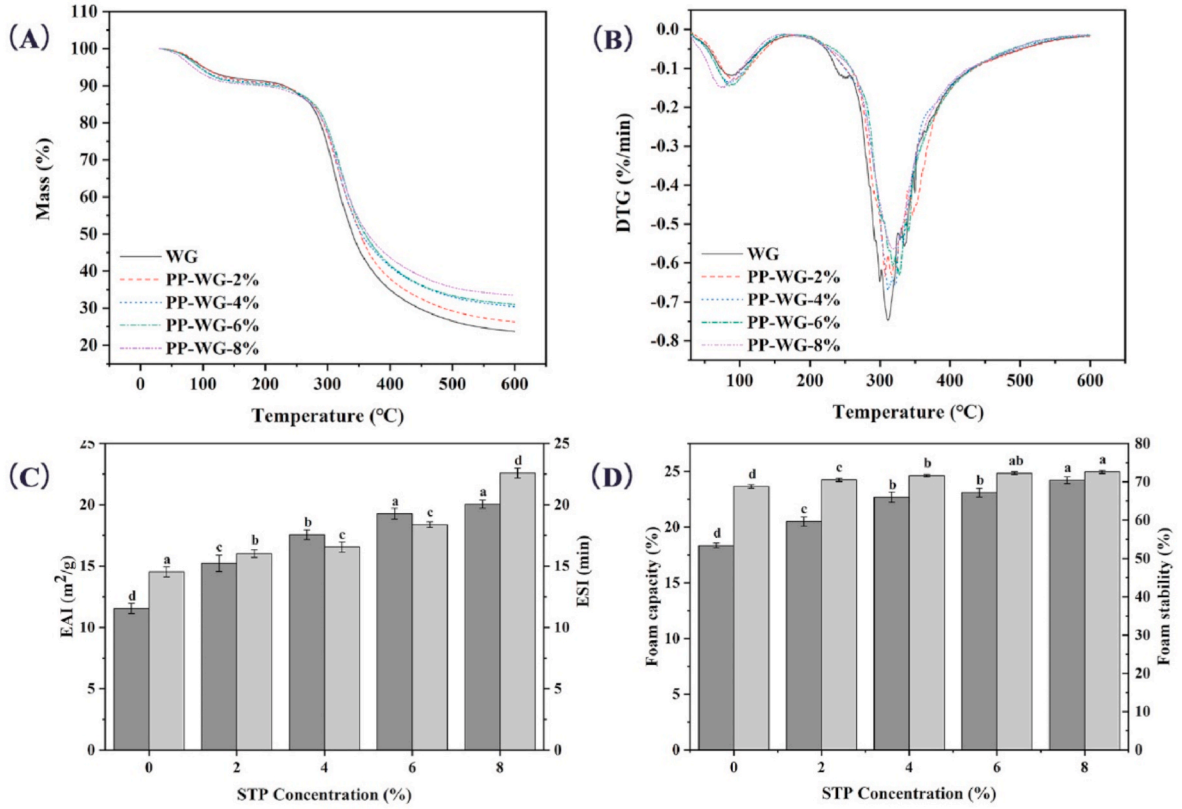

Fig. 5. Weight loss (A), derivative weight change (B), emulsifying activities (C) and foaming properties (D) of native and phosphorylated WG samples.

improved after phosphorylation modification.

3.10. Solubility

Having a larger hydrophobic region of action WG within molecule had not satisfied the needs of processing, therefore limiting industrial application. As shown in Table 1, the solubility of protein for phosphorylated WG remarkably increased compared to the raw WG ($p < 0.05$). Especially, comparing to the raw WG (8.53%), the protein solubility of PP-WG-8% sample (40.54%) was approximately five times higher than it. This was attributed to the fact that the polar phosphate groups of phosphorylated WG boosted the hydration of protein, leading to the improvement of solubility (J. H. Li et al., 2021). Furthermore, the electronegativity of protein solution system for phosphorylated WG increased owing to the introduction of many phosphoric acid groups, resulting in the enhancement of electrostatic repulsion, which made them prone to disperse due to mutually repulsive in solution system. This was consistent with previous researches that phosphorylation modifications increased the solubility of peanut and soybean (Sanchez-Resendiz et al., 2018).

Table 1
Solubility, WHC and OAC of native and phosphorylated WG samples.

Sample	Solubility (%)	WHC (g water/g protein)	OAC (g oil/g protein)
WG	8.53 ± 0.46^{e}	1.22 ± 0.02^{d}	1.44 ± 0.03^{d}
PP-WG-2%	16.60 ± 0.38^{d}	1.46 ± 0.02^{c}	1.58 ± 0.05^{c}
PP-WG-4%	28.55 ± 0.41^{c}	1.48 ± 0.02^{bc}	1.67 ± 0.03^{b}
PP-WG-6%	36.53 ± 0.45^{b}	1.55 ± 0.02^{ab}	1.73 ± 0.06^{ab}
PP-WG-8%	40.54 ± 0.37^{a}	1.56 ± 0.02^{a}	1.77 ± 0.03^{a}

The values 2–8% corresponds to the degree of phosphorylating agent used. The alphabetic letters (a-e) superscript letters indicate significant difference ($p < 0.05$).

3.11. WHC and OAC

The WHC and OAC of WG before and after phosphorylation were included in Table 1. WHC value of raw WG was lower than these of phosphorylated WG samples ($p < 0.05$). Furthermore, the WHC value for phosphorylated WG increased together with the concentration of STP. Protein with high water holding capacity required that it had the ability to keep hydrated. The introduction of phosphoric acid groups, which were polar, enhanced the hydration. In addition, the higher zeta potential of phosphorylated WG reinforced the electrostatic repulsion of proteins, making that the protein molecule became loose, and allowing more water to access the interior of proteins. Comparing to the hydration layer formed on the surface of proteins, the hydration layer inside molecule can be less susceptible to damage and more capable of retaining water. Table 1 included data on the oil absorption capacity of WG. It had increased by 23% ($p < 0.05$) after phosphorylation modification. The phosphorylation modification might have led to the exposure of the hidden hydrophobic groups inside protein, which was related with the increased retention of oil. Furthermore, similarly results were observed, which had reported elsewhere (S. H. Li et al., 2020).

3.12. Emulsifying properties

The EAI and ESI of phosphorylated WG were shown in Fig. 5C. The results of figure that the values of EAI for phosphorylated WG samples (15.23–20.05 m^2/g) were higher than raw WG (11.56 m^2/g), suggesting that phosphorylation modification significantly increased the emulsification activity of WG. The improvement of EAI may be related to the rough and porous structure as confirmed by SEM images, making that protein effectively and rapidly adsorbed to the oil-water interface during the process of high shear. Furthermore, phosphorylation modification can allow protein to move to the oil-water interface at high speed due to the reduction of particle size for phosphorylated WG, thereby improving

protein adsorption and oil droplet dispersion on the oil-water interface layer. In addition, the introduction of phosphoric acid groups significantly enhanced the electronegativity of protein surface and polarity, resulting in the increase of electrostatic repulsion between droplets which could play a role in preventing reaggregation inside the oil droplets. This was similarly with the reported result of Hu et al. (2019), who found that the increase of EAI in rice bran protein modified by STP had improved water solubility and hydrophobic protein surface.

ESI values significantly increased ($p < 0.05$) for phosphorylated WG samples (16.76–22.59 min) compared to raw WG (14.53 min) (Fig. 5C). ESI of proteins was the ability to remain dispersed without agglomeration, flocculation and emulsification, which was positively correlated with solubility and protein surface charge. The increase of ESI in phosphorylated WG might be consequence of the higher solubility of protein and the enhancement of the intermolecular electrostatic repulsion between droplets. In addition, the introduction of negative charges in phosphorylated WG greatly reduced the surface tension of emulsion, making it easier to disperse and to form emulsion droplets. In conclusion, the EAI and ESI of WG were improved by phosphorylation modification of STP.

3.13. Foaming properties

The changes of the FC and FS of WG after phosphorylation modification were displayed in Fig. 5D. It can be seen from figure that the FC (20.51–24.22%) and FS (70.55–72.62%) of phosphorylated WG samples had been improved remarkably compared to the raw WG ($p < 0.05$). Generally, the FC and FS of WG varied with the solubility of WG, as some of peptide chains stretched at the interface and formed a two-dimensional protective network through intra- and intermolecular interactions, making interfacial film to be strengthened, thus promoting the formation and stability of foam. The increase of FC and FS in phosphorylated WG may be attributed to the improvement of protein solubility, which facilitated more proteins to migrate to the air-water interface, thereby leading to forming more bubbles and boosting the trend of foam fabricating and stabilizing. Moreover, the increase in zeta potential of WG by phosphorylation modification can boost the electrostatic repulsion and surface hydrophobicity of proteins, thus enhancing the inter-molecular (protein-protein) interaction and inhibiting the aggregation of bubbles. These results were consistent with the findings by Wang et al. (2019), which reported that foam properties of rice glutenin were improved by phosphorylation.

4. Conclusion

WG was phosphorylated and its properties were investigated with complementary spectroscopy techniques, microscopy and other tests that informed about its behavior in solution. XPS and FTIR analysis evidenced that the WG could be phosphorylated through the binding between the phosphoric acid groups of sodium tripolyphosphate and –OH or $–NH_2$ groups of protein by covalent interactions (C–O–P and C–N–P bonds). Phosphorylation reduced the protein crystal size and new bonds were formed in protein according to XRD. Parts of its surface was rather irregular according to SEM analysis. Through phosphorylation modification, many negatively charged phosphoric acid groups were introduced to the surface of proteins, which resulted in an increase of zeta potential. This was likely to create a strong enough electrostatic repulsion between droplets to provide better spatial stability and prevent aggregation between droplets. Comparing to raw WG, particle size of phosphorylated WG had narrower distribution and smaller average particle size. Furthermore, the protein structure was unfolded and showed greater flexibility, transforming from an initially insoluble WG agglomerates to a soluble component by phosphorylation. The change in WG structure after phosphorylation facilitated the combination between the water and proteins, thereby increasing the solubility of protein and further improving physicochemical characteristics of WG involving emulsification, foaming, rheological properties, and thermal stability. Therefore, phosphorylation is a method that can improve functional characteristics of WG and help to expand its applications in the biomedical and food science.

CRediT authorship contribution statement

Fei Hu: Supervision, Investigation, Writing – original draft, All the authors listed above have read and approved to the version of the final manuscript. **Peng-Ren Zou:** Investigation, Methodology, All the authors listed above have read and approved to the version of the final manuscript. **Fan Zhang:** Formal analysis, Conceptualization, All the authors listed above have read and approved to the version of the final manuscript. **Kiran Thakur:** Writing – original draft, Writing – review & editing, All the authors listed above have read and approved to the version of the final manuscript. **Mohammad Rizwan Khan:** Conceptualization, All the authors listed above have read and approved to the version of the final manuscript. **Rosa Busquets:** Writing – review & editing, All the authors listed above have read and approved to the version of the final manuscript. **Jian-Guo Zhang:** Resources, Software, All the authors listed above have read and approved to the version of the final manuscript. **Zhao-Jun Wei:** Resources, Writing – original draft, Writing – review & editing, All the authors listed above have read and approved to the version of the final manuscript.

Declaration of competing interest

The authors declare that they have no known competing financial interests or personal relationships that could have appeared to influence the work reported in this paper.

Acknowledgement

This study was supported by the Key Research and Development Projects of Anhui Province (202104f06020026, 202004a06020042, 202004a06020052, 201904a06020008), the Researchers Supporting Project King Saud University (Riyadh, Saudi Arabia) (RSP-2021/138).

References

Abedi, E., Pourmohammadi, K., 2021. Chemical modifications and their effects on gluten protein: an extensive review. Food Chem. 343, 1–16. https://doi.org/10.1016/j.foodchem.2020.128398.

Ai, M.M., Jiang, A.M., 2021. Phosphorylation modification affects the gelation behavior of alkali-induced duck egg white gels. Food Chem. 340, 1–11. https://doi.org/10.1016/j.foodchem.2020.128185.

Arte, E., Huang, X., Nordlund, E., Katina, K., 2019. Biochemical characterization and technofunctional properties of bioprocessed wheat bran protein isolates. Food Chem. 289, 103–111. https://doi.org/10.1016/j.foodchem.2019.03.020.

Chai, Tsun-Thai, , Shin-Yii Ang, Goh, Kervine, Lee, You-Han, Ngoo, Jia-Min, Teh, Lai-Kuan, Wong, Fai-Chu, 2020. Trypsin-hydrolyzed corn silk proteins: antioxidant activities, in vitro gastrointestinal and thermal stability, and hematoprotective effects. eFood 1 (2), 156–164. https://doi.org/10.2991/efood.k.200323.001.

Chen, J.Y., Ren, Y.X., Zhang, K.S., Xiong, Y.L.L., Wang, Q., Shang, K., Zhang, D., 2020. Site-specific incorporation of sodium tripolyphosphate into myofibrillar protein from mantis shrimp (*Oratosquilla oratoria*) promotes protein crosslinking and gel network formation. Food Chem. 312, 9.

D'Amico, S., Maschle, J., Jekle, M., Tomoskozi, S., Lango, B., Schoenlechner, R., 2015. Effect of high temperature drying on gluten-free pasta properties. LWT–Food Sci. Technol. 63 (1), 391–399. https://doi.org/10.1016/j.lwt.2015.03.080.

Duarte, L.G.R., Alencar, W.M.P., Iacuzio, R., Silva, N.C.C., Picone, C.S.F., 2022. Synthesis, characterization and application of antibacterial lactoferrin nanoparticles. Curr. Res. Food Sci. 5, 642–652. https://doi.org/10.1016/j.crfs.2022.03.009.

Farooq, S., Ahmad, M.I., Abdullah, 2022. Interfacial rheology of sodium caseinate/high acyl gellan gum complexes: stabilizing oil-in-water emulsions. Curr. Res. Food Sci. 5, 234–242. https://doi.org/10.1016/j.crfs.2022.01.012.

Gultekin Subasi, Busra, Xiao, Jianbo, Capanogluo, Esra, 2021. Potential use of Janus structures in food applications. eFood 2 (6), 279–287. https://doi.org/10.53365/efood.k/146162.

Hadidi, M., Jafarzadeh, S., Ibarz, A., 2021. Modified mung bean protein: optimization of microwave-assisted phosphorylation and its functional and structural characterizations. LWT–Food Sci. Technol. 151, 1–9. https://doi.org/10.1016/j.lwt.2021.112119.

He, W.M., Yang, R.J., Zhao, W., 2019. Effect of acid deamidation-alcalase hydrolysis induced modification on functional and bitter-masking properties of wheat gluten hydrolysates. Food Chem. 277, 655–663. https://doi.org/10.1016/j.foodchem.2018.11.004.

Hu, Z.Y., Qiu, L., Sun, Y., Xiong, H., Ogra, Y., 2019. Improvement of the solubility and emulsifying properties of rice bran protein by phosphorylation with sodium trimetaphosphate. Food Hydrocolloids 96, 288–299. https://doi.org/10.1016/j.foodhyd.2019.05.037.

Hu, Y.P., Zhang, L., Yi, Y.W., Solangi, I., Zan, L.S., Zhu, J., 2021. Effects of sodium hexametaphosphate, sodium tripolyphosphate and sodium pyrophosphate on the ultrastructure of beef myofibrillar proteins investigated with atomic force microscopy. Food Chem. 338, 8. https://doi.org/10.1016/j.foodchem.2020.128146.

Li, C.P., Hayashi, Y., Enomoto, H., Hu, F.Y., Sawano, Y., Tanokura, M., Aoki, T., 2009. Phosphorylation of proteins by dry-heating in the presence of pyrophosphate and some characteristics of introduced phosphate groups. Food Chem. 114 (3), 1036–1041. https://doi.org/10.1016/j.foodchem.2008.10.066.

Li, P.S., Jin, Y.G., Sheng, L., 2020. Impact of microwave assisted phosphorylation on the physicochemistry and rehydration behaviour of egg white powder. Food Hydrocolloids 100, 1–8. https://doi.org/10.1016/j.foodhyd.2019.105380.

Li, S.H., Qu, Z.H., Feng, J., Chen, Y., 2020. Improved physicochemical and structural properties of wheat gluten with konjac glucomannan. J. Cereal. Sci. 95, 1–7. https://doi.org/10.1016/j.jcs.2020.103050.

Li, J.H., Wang, J., Zhai, J.L., Gu, L.P., Su, Y.J., Chang, C.H., Yang, Y.J., 2021. Improving gelling properties of diluted whole hen eggs with sodium chloride and sodium tripolyphosphate: study on intermolecular forces, water state and microstructure. Food Chem. 358, 8. https://doi.org/10.1016/j.foodchem.2021.129823.

Li, X.Y., Shi, J., Scanlon, M., Xue, S.J., Lu, J., 2021. Effects of pretreatments on physicochemical and structural properties of proteins isolated from canola seeds after oil extraction by supercritical-CO_2 process. LWT–Food Sci. Technol. 137, 1–9. https://doi.org/10.1016/j.lwt.2020.110415.

Li, D.D., Wei, Z.H., Sun, J.L., Xue, C.H., 2022. Tremella polysaccharides-coated zein nanoparticles for enhancing stability and bioaccessibility of curcumin. Curr. Res. Food Sci. 5, 611–618. https://doi.org/10.1016/j.crfs.2022.03.008.

Liu, B.Y., Li, Z.N., Zhang, J.S., Du, M., Fang, F., Chen, F.S., 2021. An environment-friendly wood adhesive using modified wheat gluten by isophorone diisocyanate. Ind. Crop. Prod. 173, 1–7. https://doi.org/10.1016/j.indcrop.2021.114125.

Marangoni, L., Rodrigues, P.R., da Silva, R.G., Vieira, R.P., Alves, R.M.V., 2022. Improving the mechanical properties and thermal stability of sodium alginate/hydrolyzed collagen films through the incorporation of SiO_2. Curr. Res. Food Sci. 5, 96–101. https://doi.org/10.1016/j.crfs.2021.12.012.

Ortolan, F., Urbano, K., Netto, F.M., Steel, C.J., 2022. Chemical and structural characteristics of proteins of non-vital and vital wheat glutens. Food Hydrocolloids 125, 1–10. https://doi.org/10.1016/j.foodhyd.2021.107383.

Rombouts, I., Lagrain, B., Lamberts, L., Celus, I., Brijs, K., Delcour, J.A., 2019. Wheat gluten amino acid analysis by high-performance anion-exchange chromatography with integrated pulsed amperometric detection. Methods Mol. Biol. 2030, 381–394. https://doi.org/10.1016/j.chroma.2009.05.066.

Sanchez-Resendiz, A., Rodriguez-Barrientos, S., Rodriguez-Rodriguez, J., Barba-Davila, B., Serna-Saldivar, S.O., Chuck-Hernandez, C., 2018. Phosphoesterification of soybean and peanut proteins with sodium trimetaphosphate (STMP): changes in structure to improve functionality for food applications. Food Chem. 260, 299–305. https://doi.org/10.1016/j.foodchem.2018.04.009.

Shamsudin, N.A., Low, Y.K., Cheng, L.H., 2022. Effects of glucono delta lactone dipping and in-pack pasteurization on rice noodles properties. Curr. Res. Food Sci. 5, 886–891. https://doi.org/10.1016/j.crfs.2022.05.007.

Shi, L.F., Fu, X., Tan, C.P., Huang, Q., Zhang, B., 2017. Encapsulation of ethylene gas into granular cold-water-soluble starch: structure and release kinetics. J. Agric. Food Chem. 65 (10), 2189–2197. https://doi.org/10.1016/j.carbpol.2022.119360.

Shi, Xiao-Dan, Huang, Jing-Jing, Han, Jin-Zhi, Wang, Shao-Yun, 2021. Physicochemical and functional properties of starches from pachyrhizus erosus with low digestibility. eFood 2 (3), 154–161. https://doi.org/10.2991/efood.k.210626.001.

Wang, J., 2020. Exploring cereal functions: a profile of Wang Jing. Food Frontiers 1, 205–207. https://doi.org/10.1002/fft2.17.

Wang, L., Wu, M., Liu, H.M., 2017. Emulsifying and physicochemical properties of soy hull hemicelluloses-soy protein isolate conjugates. Carbohydr. Polym. 163, 181–190. https://doi.org/10.1016/j.carbpol.2017.01.069.

Wang, Y.Q., Gan, J., Zhou, Y., Cheng, Y.Q., Nirasawa, S., 2017. Improving solubility and emulsifying property of wheat gluten by deamidation with four different acids: effect of replacement of folded conformation by extended structure. Food Hydrocolloids 72, 105–114. https://doi.org/10.1016/j.foodhyd.2017.04.013.

Wang, Y.R., Yang, Q., Fan, J.L., Zhang, B., Chen, H.Q., 2019. The effects of phosphorylation modification on the structure, interactions and rheological properties of rice glutelin during heat treatment. Food Chem. 297, 1–10. https://doi.org/10.1016/j.foodchem.2019.124978.

Wang, D., Zheng, X., Fan, Q., Wang, P., Zeng, H., Zhang, Y., Zheng, B., Lin, S., 2021. The effect of dynamic high-pressure microfluidization on the physicochemical and digestive properties of proteins in insoluble fraction of edible bird's nest. Food Frontiers 3, 339–346. https://doi.org/10.1002/fft2.126.

Wang, Z.M., Hao, J., Deng, Y.Y., Liu, J., Wei, Z.C., Zhang, Y., Tang, X.J., Zhou, P.F., Iqbal, Z., Zhang, M.W., Liu, G., 2021. Viscoelastic properties, antioxidant activities and structure of wheat gluten modified by rice bran. LWT–Food Sci. Technol. 150, 1–9. https://doi.org/10.1016/j.lwt.2021.112003.

Wehrli, M.C., Kratky, T., Schopf, M., Scherf, K.A., Becker, T., Jekle, M., 2021. Thermally induced gluten modification observed with rheology and spectroscopies. Int. J. Biol. Macromol. 173, 26–33. https://doi.org/10.1016/j.ijbiomac.2021.01.008.

Xiong, Z.Y., Zhang, M.J., Ma, M.H., 2016. Emulsifying properties of ovalbumin: improvement and mechanism by phosphorylation in the presence of sodium tripolyphosphate. Food Hydrocolloids 60, 29–37. https://doi.org/10.1016/j.foodhyd.2016.03.007.

Yan, C.J., Zhou, Z., 2021. Solubility and emulsifying properties of phosphorylated walnut protein isolate extracted by sodium trimetaphosphate. LWT–Food Sci. Technol. 143, 1–10. https://doi.org/10.1016/j.lwt.2021.111117.

Yang, S.F., Dai, L., Mao, L.K., Liu, J.F., Yuan, F., Li, Z.G., Gao, Y.X., 2019. Effect of sodium tripolyphosphate incorporation on physical, structural, morphological and stability characteristics of zein and gliadin nanoparticles. Int. J. Biol. Macromol. 136, 653–660. https://doi.org/10.1016/j.ijbiomac.2019.06.052.

Yu, L., Yang, W.Q., Sun, J., Zhang, C.S., Bi, J., Yang, Q.L., 2015. Preparation, characterisation and physicochemical properties of the phosphate modified peanut protein obtained from *Arachin Conarachin L.* Food Chem. 170, 169–179. https://doi.org/10.1016/j.foodchem.2014.08.047.

Yu, Q., Chen, W., Zhong, J., Huang, D., Shi, W., Chen, H., Yan, C., 2022. Purification, structural characterization, and bioactivities of a polysaccharide from Coreopsis tinctoria. Food Frontiers 1–13. https://doi.org/10.1002/fft2.145.

Zhang, K.S., Li, Y.Y., Ren, Y.X., 2007. Research on the phosphorylation of soy protein isolate with sodium tripoly phosphate. J. Food Eng. 79 (4), 1233–1237. https://doi.org/10.1016/j.jfoodeng.2006.04.009.

Zhang, A.Q., He, J.L., Wang, Y., Zhang, X., Piao, Z.H., Xue, Y.T., Zhang, Y.H., 2021. Whey protein isolate modified with sodium tripolyphosphate gel: a novel pH-sensitive system for controlled release of Lactobacillus plantarum. Food Hydrocolloids 120, 8. https://doi.org/10.1016/j.foodhyd.2021.106924.

Zhao, J., Bhandari, B., Gaiani, C., Prakash, S., 2022. Altering almond protein function through partial enzymatic hydrolysis for creating gel structures in acidic environment. Curr. Res. Food Sci. 5, 653–664. https://doi.org/10.1016/j.crfs.2022.03.012.

Zhao, Q.L., Hong, X., Fan, L.P., Liu, Y.F., Li, J.W., 2022. Solubility and emulsifying properties of perilla protein isolate: improvement by phosphorylation in the presence of sodium tripolyphosphate and sodium trimetaphosphate. Food Chem. 382, 12. https://doi.org/10.1016/j.foodchem.2022.132252.

Zheng, W.-Y., Wu, X.-M., Li, M.-X., Qiu, S.-L., Yang, T.-D., Yang, R., Chen, Z.-P., Wang, S.-Y., Liao, L., 2022. Synergistic strongly coupled super-deamidation of wheat gluten by glucose-organic acid natural deep eutectic solvent and the efficaciousness of structure and functionality. Food Hydrocolloids 125, 107437. https://doi.org/10.1016/j.foodhyd.2021.107437.

Zou, P.-R., Hu, F., Ni, Z.-J., Zhang, F., Thakur, K., Zhang, J.-G., Wei, Z.-J., 2022a. Effects of phosphorylation pretreatment and subsequent transglutaminase cross-linking on physicochemical, structural, and gel properties of wheat gluten. Food Chem. 392, 133296 https://doi.org/10.1016/j.foodchem.2022.133296.

Zou, P.-R., Hu, F., Zhang, F., Thakur, K., Rizwan Khan, M., Busquets, R., Zhang, J.-G., Wei, Z.-J., 2022b. Hydrophilic co-assembly of wheat gluten proteins and wheat bran cellulose improving the bioavailability of curcumin. Food Chem. 397, 133807 https://doi.org/10.1016/j.foodchem.2022.133807.